MHD flow of nanofluids over an exponentially stretching sheet in a porous medium with convective boundary conditions

T. Hayat[a)b)†], M. Imtiaz[a)], A. Alsaedi[b)], and R. Mansoor[a)]

[a)] *Department of Mathematics, Quaid-I-Azam University, Islamabad* 44000, *Pakistan*
[b)] *Department of Mathematics, Faculty of Science, King Abdulaziz University, Jeddah* 21589, *Saudi Arabia*

(Received 29 April 2013; revised manuscript received 26 October 2013; published online 1 April 2014)

This article concentrates on the steady magnetohydrodynamic (MHD) flow of viscous nanofluid. The flow is caused by a permeable exponentially stretching surface. An incompressible fluid fills the porous space. A comparative study is made for the nanoparticles namely Copper (Cu), Silver (Ag), Alumina (Al_2O_3) and Titanium Oxide (TiO_2). Water is treated as a base fluid. Convective type boundary conditions are employed in modeling the heat transfer process. The non-linear partial differential equations governing the flow are reduced to an ordinary differential equation by similarity transformations. The obtained equations are then solved for the development of series solutions. Convergence of the obtained series solutions is explicitly discussed. The effects of different parameters on the velocity and temperature profiles are shown and analyzed through graphs.

Keywords: MHD nanofluid, exponentially stretching sheet, porous medium, convective boundary conditions

PACS: 47.15.–x, 47.65.–d **DOI:** 10.1088/1674-1056/23/5/054701

1. Introduction

The boundary layer flow and heat transfer over a stretching sheet have momentous aspects not only from a theoretical point of view but also regarding their practical applications in the polymer industry, paper production, food processing, crystal growing etc. The rate of heat transfer between the stretching surface and fluid flow is important for the end product's desired quality. The boundary layer flow generated by a stretching sheet was first studied by Crane.[1] He constructed an exact solution for the arising problem. Afterwards, the boundary layer flows by linear and nonlinear stretching surfaces have attracted a great deal of attention of the researchers.[2–5] Some investigations in the past dealt with the flow induced by an exponentially stretching surface. Magyari and Keller[6] discussed the steady boundary layer flow by an exponentially stretching surface with an exponential temperature distribution. The effect of viscous dissipation in the mixed convection flow due to an exponentially stretching sheet has been examined by Partha *et al.*[7] Sajid and Hayat[8] studied the thermal radiation effects on the flow due to an exponentially stretching sheet. They developed the analytic solution for the resulting problem. A numerical solution for the same problem was given by Bidin and Nazar.[9] MHD boundary layer flow due to an exponentially stretching sheet with a radiation effect has been obtained by Anuar Ishak.[10] Bachok *et al.*[11] studied the boundary layer stagnation-point flow and heat transfer over an exponentially stretching/shrinking sheet. The boundary layer flow over an exponentially stretching porous sheet with heat flux in a porous medium has been obtained by Mandal and Mukhopadhyay.[12] Bhattacharyya[13] discussed the steady boundary layer flow and reactive mass transfer past an exponentially stretching surface in an exponentially moving free stream. Elbashbeshy[14] studied the effects of thermal radiation and magnetic field on unsteady mixed convection flow and heat transfer over an exponentially stretching surface with suction in the presence of internal heat generation/absorption. Boundary layer flow and heat transfer over an exponentially shrinking vertical sheet with suction was analyzed by Azizah Mohd Rohni.[15] Mukhopadhyay[16] studied the MHD boundary layer flow and heat transfer over an exponentially stretching sheet embedded in a thermally stratified medium.

As oil, water and ethylene glycol mixtures are poor heat transfer fluids, they therefore have low thermal conductivities. Since the thermal conductivity of fluids plays an important role in the heat transfer coefficient, so many methods have been used to enhance the thermal conductivity of fluids. However, it is observed that enhancement of the thermal conductivity of poor heat transfer fluids is possible in view of the addition of nanoparticles in the base fluids. The nano particles can be found in metals such as (Cu, Ag), oxides (Al_2O_3), carbides (SiC), nitrides (AlN, SiN) or nonmetals (graphite, carbon nanotubes). Nanofluids have novel properties that make them potentially useful in many applications in heat transfer including microelectronics, fuel cells, pharmaceutical processes and hybrid-powered engines. Nanoparticles provide a bridge between bulk materials and molecular structure. The term "nanofluid" was first introduced by Choi.[17] Recently many investigations regarding nanofluids have been reported[18–21] Narayana and Sibanda[22] studied the effects of laminar flow

†Corresponding author. E-mail: pensy_t@yahoo.com

© 2014 Chinese Physical Society and IOP Publishing Ltd

of a nanoliquid film over an unsteady stretching sheet. Thermophysical properties of nanofluids such as thermal conductivity, diffusivity and viscosity have been studied by Kang *et al.*,[23] Velagapudi *et al.*[24] and Rudyak *et al.*[25] Boundary layer flow of nanofluid past a stretching sheet with convective boundary condition was studied by Makinde and Aziz.[26] Alsaedi *et al.*[27] studied the effects of heat generation/ absorption in stagnation point flow of a nanofluid over a linearly stretching surface with convective boundary conditions. Recently, Kandasamy[28] investigated the unsteady Hiemenz flow of Cu-nanofluid over a porous wedge in the presence of thermal stratification. Kameswaran *et al.*[29] examined the homogeneous–heterogeneous reactions in a nanofluid flow due to a porous stretching sheet. Mustafa *et al.*[30] addressed the stagnation point flow of a viscous nanofluid towards a linear stretching sheet. Nandy and Mahapatra[31] studied the effects of slip and heat generation/absorption in MHD stagnation point flow of a nanofluid past a stretching/shrinking surface with convective boundary conditions. Ibrahim[32] analyzed the MHD stagnation point flow and heat transfer in a nanofluid towards a stretching sheet. Makinde[33] examined the buoyancy effects on MHD stagnation point flow and heat transfer of a nanofluid past a convectively heated stretching/shrinking sheet. MHD boundary layer flow and heat transfer of a nanofluid past a permeable stretching sheet with velocity, thermal and solutal slip boundary conditions has been analyzed by Ibrahim.[34] Zheng *et al.*[35] studied the flow and radiation heat transfer of a nanofluid over a stretching sheet with velocity slip and temperature jump in a porous medium. The effects of a magnetic field on the radiative flow of a nanofluid past a stretching sheet have been examined by Khan.[36]

The magnetic nanofluids are important to guide the particles up the bloodstream to a tumor with magnets. In fact, magnetic nanoparticles are more adhesive to tumor cells than nano-malignant cells and therefore absorb much more power than microparticles in alternating current magnetic fields tolerable in humans. No doubt, the magnetic nanoparticles have broad interest in medicine, in sink float separation and the construction of loudspeakers. Besides this, the heat transfer in a porous medium is significant in geothermal reservoirs, thermal insulation, nuclear reactors, underground energy transport etc. Hence, the present article is arranged to investigate the boundary layer flow of a magneto nanofluid in a porous medium. Exponentially permeable stretched surfaces possess the convective type boundary conditions. In fact, the nanoparticles are used to enhance the thermal conductivity of the fluid. On the other hand, the convective boundary condition in dimensionless form appears as a Biot number. An increase in the Biot number raises the temperature. An increase in temperature corresponds to an enhancement in the thermal conductivity. So the nanofluid with a convective boundary condition is a more appropriate model in comparison to the constant surface temperature conditions. This article is structured as follows.

Section 2 consists of the problem formulation. Sections 3 and 4 develop the analysis for the series solutions by the homotopy analysis method (HAM)[37–40] and related convergence domains. Discussion to various influential parameters is also made in Section 4. The conclusions are given in Section 5.

2. Model development

Let us consider the steady and two-dimensional flow of an incompressible nanofluid induced by an exponentially stretching surface in a porous medium with permeability K (Fig. 1). The x axis is taken along the stretching surface in the direction of motion and the y axis is perpendicular to it.

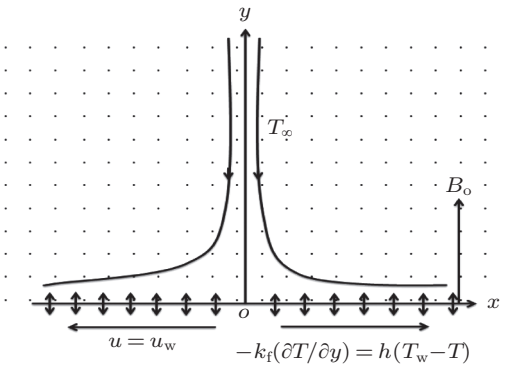


Fig. 1. Geometry of the problem.

A uniform transverse magnetic field of strength B_o is applied parallel to the y axis. It is assumed that the induced magnetic field and the electric field effects are negligible. Further, the surface exhibits convective type boundary conditions. The boundary layer flow in the present analysis is governed by the following equations:

$$\frac{\partial u}{\partial x}+\frac{\partial v}{\partial y}=0, \tag{1}$$

$$\rho_{nf}\left(u\frac{\partial u}{\partial x}+v\frac{\partial u}{\partial y}\right)=\mu_{nf}\frac{\partial^2 u}{\partial y^2}-\frac{\mu_{nf}}{K}u-\sigma B_o^2 u, \tag{2}$$

$$u\frac{\partial T}{\partial x}+v\frac{\partial T}{\partial y}=\frac{k_{nf}}{(\rho C_p)_{nf}}\frac{\partial^2 T}{\partial y^2}, \tag{3}$$

where u and v are the velocity components along the x and y directions respectively, and σ is the electrical conductivity of the fluid. The effective density ρ_{nf}, the effective dynamic viscosity μ_{nf}, the heat capacitance $(\rho C_p)_{nf}$ and the thermal conductivity k_{nf} of the nanofluid are given by

$$\rho_{nf}=\rho_f(1-\phi)+\rho_s\phi, \tag{4}$$

$$\mu_{nf}=\frac{\mu_f}{(1-\phi)^{2.5}}, \tag{5}$$

$$(\rho C_p)_{nf}=(\rho C_p)_f(1-\phi)+(\rho C_p)_s\phi, \tag{6}$$

$$\frac{k_{nf}}{k_f}=\frac{k_s+2k_f-2\phi(k_f-k_s)}{k_s+2k_f+2\phi(k_f-k_s)}. \tag{7}$$

Here ϕ is the solid volume fraction, subscript s is for nano-solid-particles, and subscript f is for base fluid. Graphically, the present consideration of nanofluid model is significant for a comparative study of different nanoparticles. The present model is useful for a comparative study of different nanoparticles. In the present model, the preference can be tackled through Eqs. (4)–(7). The nanoparticles are assumed to have uniform shape and size. The subjected boundary conditions are

$$\begin{aligned} &u = u_{\rm w} = U_{\rm o}\,{\rm e}^{x/L}, \quad v = v_{\rm w},\\ &-k_f\frac{\partial T}{\partial y} = h(T_{\rm w} - T), \quad \text{as} \quad y = 0,\\ &u \to 0, \ T \to T_\infty, \quad \text{as} \ y \to \infty. \end{aligned} \tag{8}$$

Introducing

$$\begin{aligned} &\eta = y\sqrt{\frac{U_{\rm o}}{2\nu_f L}}\,{\rm e}^{x/2L}, \quad u = U_{\rm o}\,{\rm e}^{x/L} f'(\eta),\\ &v = -\sqrt{\frac{\nu_f U_{\rm o}}{2L}}\,{\rm e}^{x/2L}\left[f(\eta) + \eta f'(\eta)\right],\\ &\theta(\eta) = \frac{T - T_\infty}{T_f - T_\infty}. \end{aligned} \tag{9}$$

Equation (1) is satisfied automatically and equations (2) and (3) after using Eqs. (4)–(7) can be reduced as follows:

$$\begin{aligned} &f''' + A_1(1-\phi)^{2.5}(ff'' - 2f'^2)\\ &-\lambda f' - (1-\phi)^{2.5} M f' = 0, \end{aligned} \tag{10}$$

$$\frac{1}{Pr}\theta'' + \frac{A_2}{A_3} f\theta' = 0, \tag{11}$$

$$\begin{aligned} &f'(0) = 1, \ f(0) = \alpha, \ \theta'(0) = -\gamma[1 - \theta(0)],\\ &f'(\infty) = 0, \ \theta(\infty) = 0, \end{aligned} \tag{12}$$

in which prime indicates the differentiation with respect to η and the values of A_i $(i = 1, 2, 3)$ are

$$A_1 = \frac{\rho_{\rm nf}}{\rho_f} = (1-\phi) + \frac{\rho_{\rm s}}{\rho_f}\phi, \tag{13}$$

$$A_2 = \frac{(\rho C_{\rm p})_{\rm nf}}{(\rho C_{\rm p})_f} = (1-\phi) + \frac{(\rho C_{\rm p})_{\rm s}}{(\rho C_{\rm p})_f}\phi, \tag{14}$$

$$A_3 = \frac{k_{\rm nf}}{k_f} = \frac{k_{\rm s} + 2k_f - 2\phi(k_f - k_{\rm s})}{k_{\rm s} + 2k_f + 2\phi(k_f - k_{\rm s})}. \tag{15}$$

Moreover the porosity parameter λ, the Hartman number M, the Prandtl number Pr, the mass transfer parameter with $\alpha > 0$ for suction on and $\alpha < 0$ for injection and the Biot number γ are defined as follows:

$$\begin{aligned} &\lambda = \frac{\nu_f L}{K U_{\rm o}}\,{\rm e}^{-x/L}, \ M = \frac{2\sigma B_{\rm o}^2 L}{\rho_f U_{\rm o}}\,{\rm e}^{-x/L}, \quad Pr = \frac{\nu_f (\rho C_P)_f}{k_f},\\ &\alpha = -\sqrt{\frac{2L}{\nu U_{\rm o}}}\,{\rm e}^{-x/2L} v_{\rm w}, \quad \gamma = \frac{h}{k_f}\sqrt{\frac{\nu_f}{a}}. \end{aligned} \tag{16}$$

Local skin-friction coefficient C_f and local Nusselt number Nu are given by

$$C_f = \frac{2\tau_{\rm w}|_{y=0}}{\rho U_0^2\,{\rm e}^{\frac{2x}{L}}}, \quad Nu = -\frac{x}{(T_{\rm w} - T_\infty)}\left.\frac{\partial T}{\partial y}\right|_{y=0}, \tag{17}$$

$$C_f\sqrt{\frac{Re_x}{2}} = f''(0), \quad Nu Re_x^{-1/2}\sqrt{\frac{2L}{x}} = -\theta'(0), \tag{18}$$

in which $Re_x = U_0\,{\rm e}^{x/L} x/\nu$ denotes the local Reynolds number.

3. Solutions derivation

3.1. Zeroth-order deformation problems

We choose the initial guesses $f_{\rm o}(\eta)$ and $\theta_{\rm o}(\eta)$ and the linear operators $\mathcal{L}_1$ and $\mathcal{L}_2$ in the forms

$$\begin{aligned} &f_{\rm o}(\eta) = 1 + \alpha - \exp(-\eta),\\ &\theta_{\rm o}(\eta) = \frac{\gamma}{1+\gamma}\exp(-\eta), \end{aligned} \tag{19}$$

$$\mathcal{L}_1(f) = f''' - f', \quad \mathcal{L}_2(\theta) = \theta'' - \theta, \tag{20}$$

together with the properties

$$\begin{aligned} &\mathcal{L}_1\left[C_1 + C_2\exp(\eta) + C_3\exp(-\eta)\right] = 0,\\ &\mathcal{L}_2\left[C_4\exp(\eta) + C_5\exp(-\eta)\right] = 0, \end{aligned} \tag{21}$$

where $C_1 - C_5$ are the constants. With Eqs. (10) and (11), the definitions of operators $\mathcal{N}_f$ and $\mathcal{N}_\theta$ can be written as

$$\begin{aligned} &\mathcal{N}_f\left[\hat{f}(\eta;p), \hat{\theta}(\eta;p)\right]\\ &= \frac{\partial^3 \hat{f}(\eta,p)}{\partial\eta^3} + A_1(1-\phi)^{2.5}\\ &\times\left(\hat{f}(\eta,p)\frac{\partial^2\hat{f}(\eta,p)}{\partial\eta^2} - 2\left(\frac{\partial\hat{f}(\eta,p)}{\partial\eta}\right)^2\right)\\ &-\lambda\frac{\partial\hat{f}(\eta,p)}{\partial\eta} - (1-\phi)^{2.5} M\frac{\partial\hat{f}(\eta,p)}{\partial\eta}, \end{aligned} \tag{22}$$

$$\begin{aligned} &\mathcal{N}_\theta[\hat{\theta}(\eta,p), \hat{f}(\eta,p)]\\ &= \frac{1}{Pr}\frac{\partial^2\hat{\theta}(\eta,p)}{\partial\eta^2} + \frac{A_2}{A_3}\hat{f}(\eta,p)\frac{\partial\hat{\theta}(\eta,p)}{\partial\eta}. \end{aligned} \tag{23}$$

We construct the zeroth order problems as follows:

$$(1-p)\mathcal{L}_1\left[\hat{f}(\eta,p) - f_{\rm o}(\eta)\right] = p h_f \mathcal{N}_f[\hat{f}(\eta,p)], \tag{24}$$

$$(1-p)\mathcal{L}_2\left[\hat{\theta}(\eta,p) - \theta_{\rm o}(\eta)\right] = p h_\theta \mathcal{N}_\theta[\hat{\theta}(\eta,p)], \tag{25}$$

$$\begin{aligned} &\hat{f}'(0,p) = 1, \ \ \hat{f}(0,p) = \alpha, \ \ \hat{f}'(\infty,p) = 0,\\ &\hat{\theta}'(0,p) = -\gamma[1 - \hat{\theta}(0,p)], \ \ \hat{\theta}(\infty,p) = 0, \end{aligned} \tag{26}$$

where h_f and h_θ are the nonzero auxiliary parameters and for $p = 0$ and $p = 1$ we have

$$\begin{aligned} &\hat{f}(\eta,0) = f_{\rm o}(\eta), \ \hat{f}(\eta,1) = f(\eta),\\ &\hat{\theta}(\eta,0) = \theta_{\rm o}(\eta), \ \hat{\theta}(\eta,1) = \theta(\eta). \end{aligned} \tag{27}$$

Note that $f_o(\eta)$ and $\theta_o(\eta)$ approach $f(\eta)$ and $\theta(\eta)$ respectively, when p has variation from 0 to 1. According to the Taylor series we have

$$\hat{f}(\eta,p) = f_o(\eta) + \sum_{m=1}^{\infty} f_m(\eta)p^m,$$
$$f_m(\eta) = \frac{1}{m!}\frac{\partial^m \hat{f}(\eta,p)}{\partial p^m}\bigg|_{p=0},$$
$$\hat{\theta}(\eta,p) = \theta_o(\eta) + \sum_{m=1}^{\infty} \theta_m(\eta)p^m,$$
$$\theta_m(\eta) = \frac{1}{m!}\frac{\partial^m \hat{\theta}(\eta,p)}{\partial p^m}\bigg|_{p=0}, \tag{28}$$

where the convergence depends upon h_f and h_θ. By proper choice of h_f and h_θ, the series (28) converge for $p = 1$ and so

$$f(\eta) = f_o(\eta) + \sum_{m=1}^{\infty} f_m(\eta),$$
$$\theta(\eta) = \theta_o(\eta) + \sum_{m=1}^{\infty} \theta_m(\eta). \tag{29}$$

3.2. m-th order deformation problems

The resulting problems at this order are given by

$$\mathcal{L}_1[f_m(\eta,p) - \chi_m f_{m-1}(\eta)] = h_f \mathcal{R}_{f,m}(\eta), \tag{30}$$
$$\mathcal{L}_2[\theta_m(\eta,p) - \chi_m \theta_{m-1}(\eta)] = h_\theta \mathcal{R}_{\theta,m}(\eta), \tag{31}$$
$$f_m(0) = f'_m(0) = f'_m(\infty) = \theta'_m(0) - \gamma\theta_m(0) = \theta_m(\infty) = 0, \tag{32}$$
$$\chi_m = \begin{cases} 0, & m \le 1, \\ 1, & m > 1, \end{cases} \tag{33}$$
$$\mathcal{R}_{f,m}(\eta) = f'''_{m-1} + A_1(1-\phi)^{2.5}\sum_{k=0}^{m-1}\left[2f'_{m-1-k}f'_k - f_{m-1-k}f''_k\right] - \lambda f'_{m-1} - (1-\phi)^{2.5}Mf'_{m-1}, \tag{34}$$
$$\mathcal{R}_{\theta,m}(\eta) = \frac{1}{Pr}\theta''_{m-1} + \frac{A_2}{A_3}\sum_{k=0}^{m-1}\theta'_{m-1-k}f_k, \tag{35}$$

where the general solutions are

$$f_m(\eta) = f^*_m(\eta) + C_1 + C_2 e^{\eta} + C_3 e^{-\eta}, \tag{36}$$
$$\theta_m(\eta) = \theta^*_m(\eta) + C_4 e^{\eta} + C_5 e^{-\eta}, \tag{37}$$

in which f^*_m and ϕ^*_m denote the special solutions.

4. Analysis of the results

4.1. Convergence of the derived series solutions

Now the solutions of Eqs. (10) and (11) subject to the boundary conditions (12) are computed by means of a homotopy analysis method. We choose auxiliary parameters $\hbar_f$ and $\hbar_\theta$ for the functions f and θ respectively. The convergence of the obtained series and the rate of the approximation for HAM strongly depend upon the values of the auxiliary parameters. For ranges of admissible values of $\hbar_f$ and $\hbar_\theta$, the $\hbar$ curves for 12th-order of approximations are plotted in Figs. 2 and 3. We can see that the permissible values for $\hbar_f$ and $\hbar_\theta$ are $-0.7 \le \hbar_f \le -0.4$ and $-0.85 \le \hbar_\theta \le -0.3$. Further, the series solutions converge in the whole region of η $(0 < \eta < \infty)$ when $\hbar_f = \hbar_\theta = -0.6$.

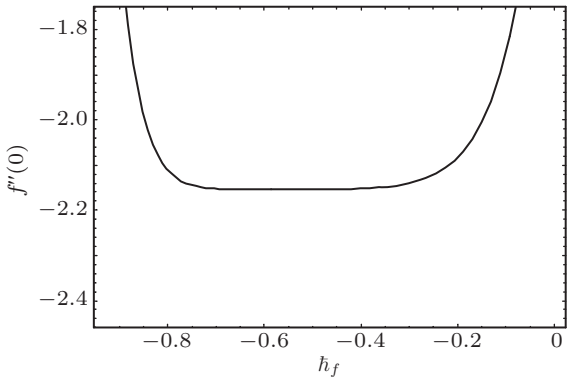


Fig. 2. The $\hbar$ curve for f. $M = 0.1$, $Pr = 1$, $\phi = 0.03$, $\gamma = 0.7$, $\alpha = 0.9$, and $\lambda = 0.5$.

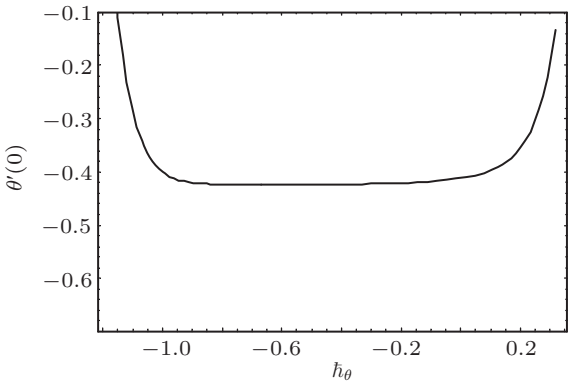


Fig. 3. The $\hbar$ curve for θ. $M = 0.1$, $Pr = 1$, $\phi = 0.03$, $\gamma = 0.7$, $\alpha = 0.9$, and $\lambda = 0.5$.

4.2. Results and discussion

In this section, we discuss the influence of various parameters on the velocity $f'(\eta)$ and temperature fields $\theta(\eta)$. Figures 4–7 are plotted to analyze the effects of volume fraction of nanoparticles (Cu), mass transfer parameter α, Hartman number M and porosity parameter λ on the velocity field f'. Effects of volume fraction of nanoparticles (Cu) on the velocity profile f' can be seen from Fig. 3. Here the values of f' and the boundary layer thickness decrease when the volume fraction for the nanoparticles increases. This is because of the fact that by increasing the volume of copper nanoparticles, the thermal conductivity increases and the boundary layer thickness decreases. The effects of the mass transfer parameter α on the velocity function f' are depicted in Fig. 4. This graph shows that the value of velocity function f' and the boundary layer thickness decrease by increasing α. Because applying suction leads to draw the amount of fluid particles into the wall and consequently the velocity boundary layer decreases.

Also suction is an agent which causes a reduction in the fluid velocity. Figure 5 shows the influence of Hartman number M on the velocity. Here we analyzed that the velocity is reduced when we increase the values of Hartman number. The application of an applied magnetic field has the tendency to slow down the movement of the fluid, which leads to a decrease in the velocity and momentum boundary layer thickness. From Fig. 6, we can see that higher values of porosity parameter λ correspond to the lower velocity. The porosity parameter depends on the permeability parameter K. An increase in the porosity parameter leads to the lower permeability parameter. This lower permeability parameter causes a reduction in the fluid velocity.

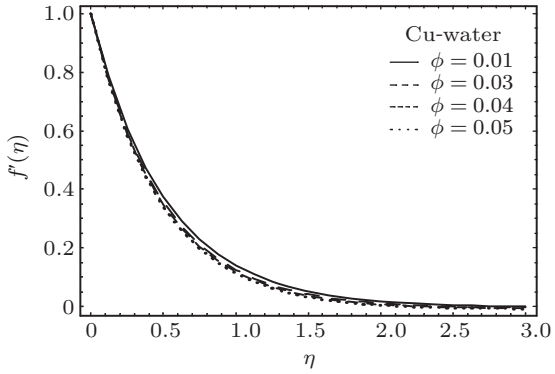


Fig. 4. Effects of ϕ on f'. $\lambda = 0.5$, $Pr = 1$, $M = 0.1$, $\alpha = 0.9$, $h = -0.6$.

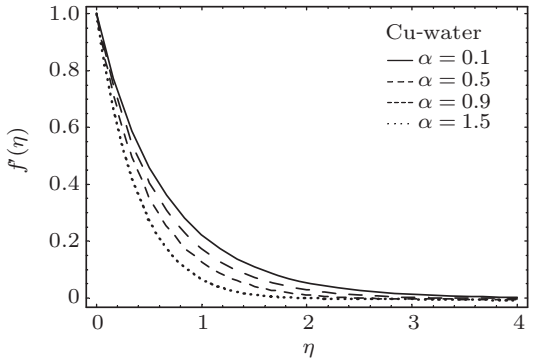


Fig. 5. Effects of α on f'. $\lambda = 0.5$, $Pr = 1$, $M = 0.1$, $\phi = 0.03$, and $h = -0.6$.

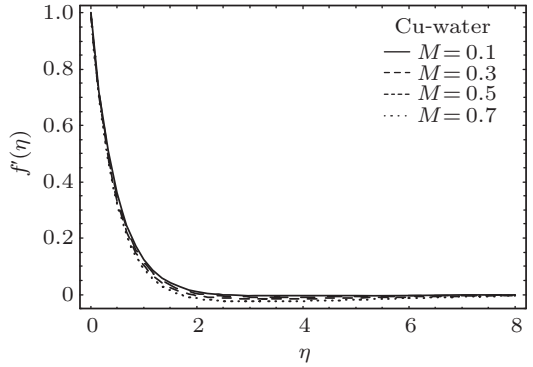


Fig. 6. Effects of M on f'. $\lambda = 0.5$, $Pr = 1$, $\alpha = 0.9$, $\phi = 0.03$, and $h = -0.6$.

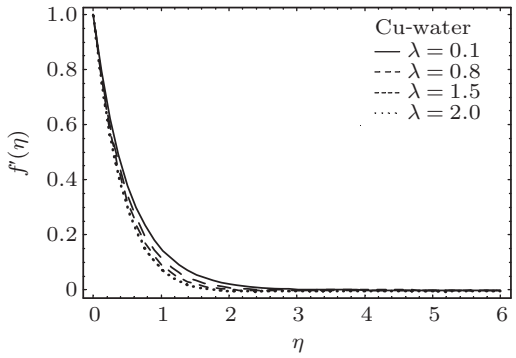


Fig. 7. Effects of λ on f'. $\alpha = 0.9$, $Pr = 1$, $M = 0.1$, $\phi = 0.03$, and $\lambda = 0.5$.

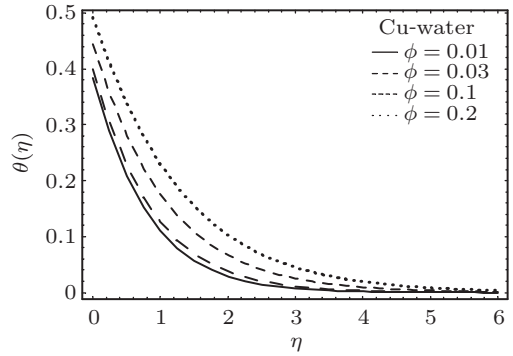


Fig. 8. Effects of ϕ on θ. $\lambda = 0.5$, $Pr = 1$, $\gamma = 0.7$, $\alpha = 0.9$, $M = 0.1$, $h = -0.6$.

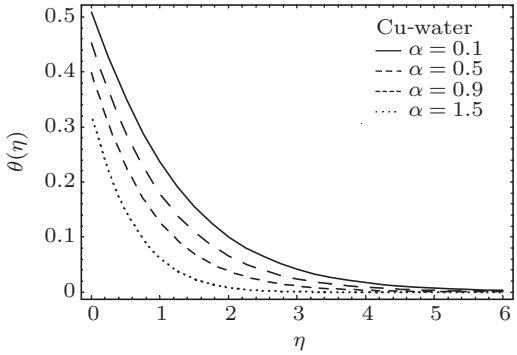


Fig. 9. Effects of α on θ. $\lambda = 0.5$, $Pr = 1$, $\gamma = 0.7$, $M = 0.1$, $\phi = 0.03$, and $h = -0.6$.

The effects of volume fraction of nanoparticles (Cu), mass transfer parameter α, Hartman number M, porosity parameter λ, Prandtl number Pr and Biot number γ on the temperature profile θ are shown in Figs. 8–13. Effect of ϕ on the temperature is analyzed in Fig. 7. It is observed that increasing the volume fraction of nanoparticles ϕ, increases the thermal conductivity of nanofluids and consequently the thermal boundary layer thickness increases. The behavior of α on the temperature profile is similar to that of the velocity profile (see Fig. 9). Figure 10 illustrates the effects of M on temperature profile θ. As the Lorentz force is a resistive force which opposes the fluid motion, so heat is produced and as a result, the thermal boundary layer thickness increases. Variations of

λ and Pr on temperature profile θ can be seen in Figs. 11–12. There is a decrease in temperature θ when porosity parameter λ and Prandtl number Pr are increased. In fact, the thermal diffusivity decreases by increasing Pr and thus the heat diffuses away slowly from the heated surface. Figure 13 represents the effect of Biot number γ on temperature profile θ. Temperature profile θ increases for an increase in γ. The Biot number involves the heat transfer coefficient. Higher values of the Biot number implies an enhancement in the heat transfer coefficient. This enhancement in the heat transfer coefficient give rise to the temperature and thermal boundary layer thickness.

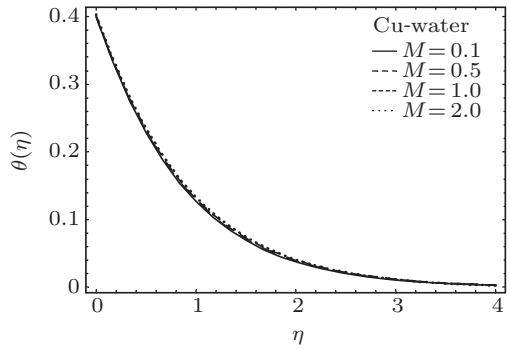


Fig. 10. Effects of M on θ. $\lambda = 0.5$, $Pr = 1$, $\gamma = 0.7$, $\alpha = 0.9$, $\phi = 0.03$, and $h = -0.6$.

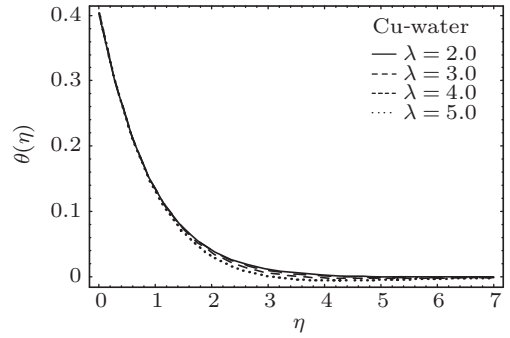


Fig. 11. Effects of λ on θ. $\phi = 0.03$, $Pr = 1$, $\gamma = 0.7$, $\alpha = 0.9$, $M = 0.1$, and $h = -0.6$.

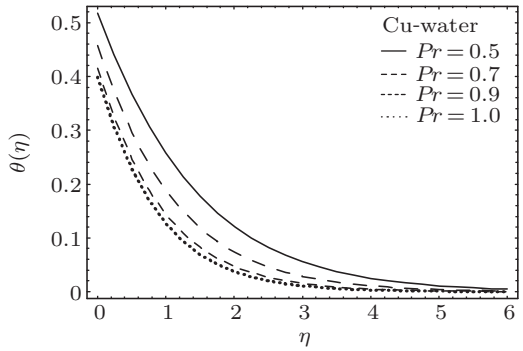


Fig. 12. Effects of Pr on θ. $\phi = 0.03$, $\lambda = 0.5$, $\gamma = 0.7$, $\alpha = 0.9$, $M = 0.1$, and $h = -0.6$.

In Figs. 14(a) and 14(b) we observe that boundary layer thickness is maximum when Alumina is chosen as the nanoparticle. Figures 15(a) and 15(b) show the effects of nanoparticle volume fraction ϕ, mass transfer parameter α and porosity parameter λ on the skin friction coefficient in the case of Cu-water. It is noticed that the skin friction coefficient decreases when we increase ϕ for both α and λ. Figures 16(a) and (16(b) describe the variation of the Nusselt number for nanoparticle volume fraction ϕ, mass transfer parameter α and porosity parameter λ. In this figure, heat transfer rates decrease as ϕ increases for both α and λ.

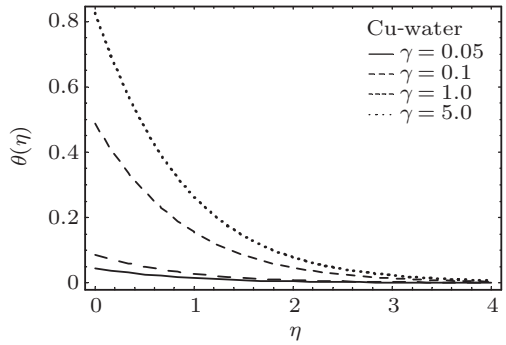


Fig. 13. Effects of γ on θ. $\phi = 0.03$, $\lambda = 0.5$, $Pr = 1$, $\alpha = 0.9$, $M = 0.1$, and $h = -0.6$.

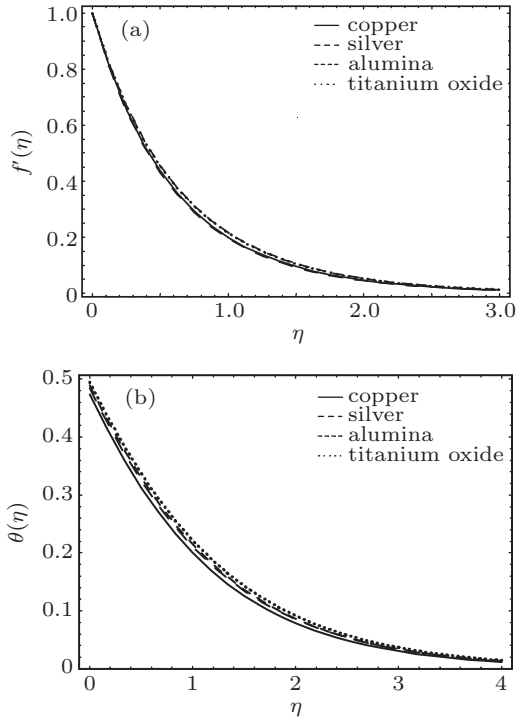


Fig. 14. (a) Velocity and (b) temperature profiles for different types of nanofluids.

Table 1 shows the convergence of the series solutions. It is observed that convergence is achieved at the 17-th order of approximations. In Table 2, some thermophysical properties of water and nanoparticles are given. Table 3 shows the effects of the nanoparticle volume fraction ϕ for different types of nanofluids on the skin friction coefficient when $\lambda = 0.5$, $M = 0.1$, and $\alpha = 0.9$. Table 4 shows the effects of the

nanoparticle volume fraction ϕ for different types of nanofluids on the Nusselt number when $\lambda = 0.5$, $Pr = 1$, $\gamma = 0.7$, $M = 0.1$, and $\alpha = 0.9$. These tables show that the shear stress and heat transfer rate change when we use different types of nanoparticles.

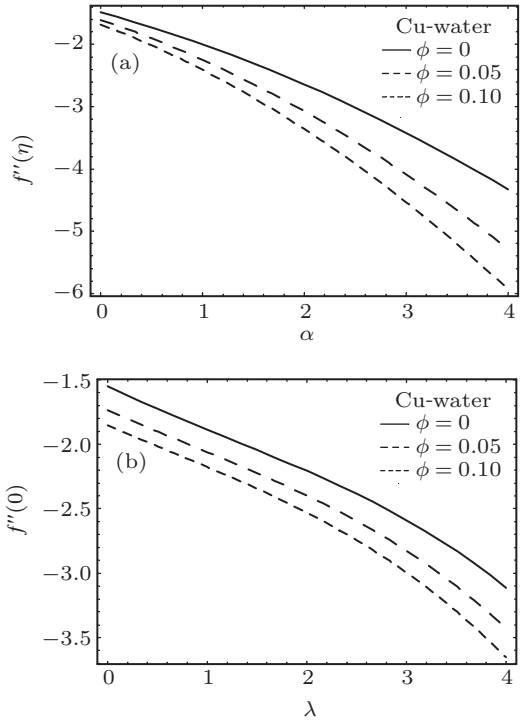


Fig. 15. (a) Effect of nanoparticle volume fraction ϕ, mass transfer parameter α and (b) porosity parameter λ on the skin friction coefficient when $M = 0.1$.

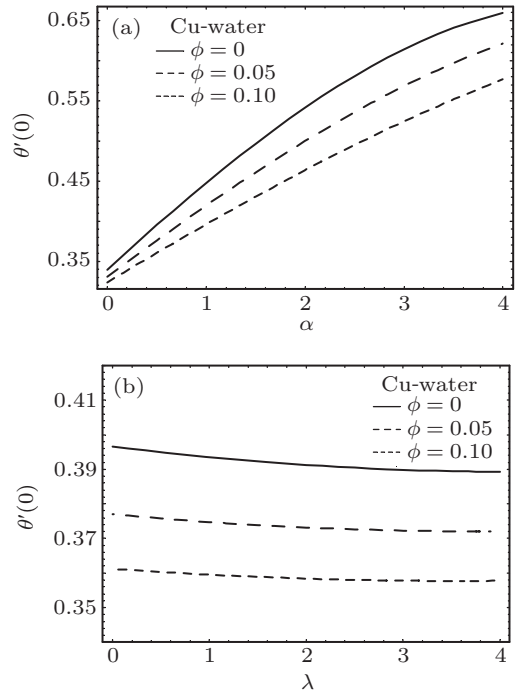


Fig. 16. Effect of nanoparticle volume fraction ϕ, (a) mass transfer parameter α and (b) porosity parameter λ on the Nusselt number when $M = 0.1$, $Pr = 1$, and $\gamma = 0.7$.

Table 1. Convergence of HAM solutions for different order of approximations when $Pr = 1$, $\phi = 0.03$, $\lambda = 0.5$, $\gamma = 0.7$, $M = 0.1$, and $\alpha = 0.9$.

Order	$-f''(0)$	$-\theta'(0)$
1	1.76172	0.416270
5	2.14446	0.422428
10	2.15409	0.423256
17	2.15426	0.423311
20	2.15426	0.423311
25	2.15426	0.423311
30	2.15426	0.423311
35	2.15426	0.423311
40	2.15426	0.423311

Table 2. Thermophysical properties of water and nanoparticles.

	ρ/kg·m^{-3}	C_p/j·kg^{-1}·k	k/W·m^{-1}·k	$\beta \times 10^5$/K^{-1}
Pure water	997.1	4179	0.613	21
Copper (Cu)	8933	385	401	1.67
Silver (Ag)	10500	235	429	1.89
Alumina (Al_2O_3)	3970	765	40	0.85
Titanium Oxide (TiO_2)	4250	686.2	8.9538	0.9

Table 3. Effect of ϕ for different types of nanofluids on the skin friction coefficient when $\lambda = 0.5$, $M = 0.1$, and $\alpha = 0.9$.

ϕ	Cu	Ag	Al_2O_3	TiO_2
0.01	−2.05387	−2.07036	−2.00143	−2.00439
0.03	−2.15426	−2.20071	−2.00558	−2.01404
0.05	−2.23960	−2.31255	−2.00535	−2.01873

Table 4. Effect of ϕ for different types of nanofluids on the Nusselt number when $\lambda = 0.5$, $Pr = 1$, $\gamma = 0.7$, $M = 0.1$, and $\alpha = 0.9$.

ϕ	Cu	Ag	Al_2O_3	TiO_2
0.01	0.436981	0.436452	0.437649	0.438380
0.03	0.423311	0.421702	0.425326	0.427566
0.05	0.409403	0.406691	0.412767	0.416582

5. Concluding remarks

Here MHD flow of nanofluid by an exponentially permeable stretching sheet is studied. The effects of different parameters on the velocity and temperature profiles are shown. A convergent approximate solution is constructed. The following observations are made.

(i) An increase in the values of ϕ, α, M and λ have similar effects on the velocity $f'(\eta)$ in a qualitative sense.

(ii) The temperature profile increases by increasing ϕ, M and γ while it decreases when α and λ are increased.

(iii) An increase in Prandtl number Pr reduces the temperature and the thermal boundary layer thickness.

(iv) The values of the skin friction coefficient are higher for increasing values of ϕ.

(v) Higher values of ϕ correspond to smaller values of the Nusselt number.

Acknowledgment

The research of Dr. Alsaedi was partially supported by the Deanship of Scientific Research (DSR), King Abdulaziz University, Jeddah, Saudi Arabia.

References

[1] Crane L J 1970 *Zeitschrift Fur Angewandte Mathematik Und Physik* **21** 645
[2] Cortell R 2006 *Phys. Lett. A* **357** 298
[3] Bhattacharyya K, Hayat T and Alsaedi A 2013 *Chin. Phys. B* **22** 024702
[4] Mukhopadhyay S 2013 *Chin. Phys. B* **22** 074701
[5] Rashidi M M and Mohimanian Pour S A 2010 *Nonlinear Analysis: Modelling and Control* **15** 83
[6] Magyari E and Keller B 1999 *J. Phys. D: Appl. Phys.* **32** 577
[7] Partha M K, Murthy P V S N and Rajasekhar G P 2005 *Heat Mass Transfer* **41** 360
[8] Sajid M and Hayat T 2008 *Int. Comm. Heat Mass Transfer* **35** 347
[9] Bidin B and Nazar R 2009 *Euro. J. Sci. Research* **33** 710
[10] Ishak A 2011 *Sains Malaysiana* **40** 391
[11] Bachok N, Ishak A and Pop I 2012 *Int. J. Heat Mass Transfer* **55** 8122
[12] Mandal I C and Mukhopadhyay S 2013 *Ain Shams Eng. J.* **4** 103
[13] Bhattacharyya K 2012 *J. Egy. Math. Society* **20** 223
[14] Elbashbeshy E M A, Emam T G and Abdelgaber K M 2012 *J. Egy. Math. Society* **20** 215
[15] Rohni A M, Ahmad S, Ismail A I M and Pop I 2013 *I. J. Ther. Sci.* **64** 264
[16] Mukhopadhyay S 2013 *Alexandria Eng. J.* **52** 259
[17] Choi S U S 1995 *ASME FED* **231** 99
[18] Buongiorno J 2006 *ASME J. Heat Transfer* **128** 240
[19] Kuznetsov A V and Nield D A 2010 *Int. J. Therm. Sci.* **49** 243
[20] Nield D A and Kuznetsov A V 2009 *Int. J. Heat Mass Transfer* **52** 5792
[21] Cheng P and Minkowycz W 1977 *J. Geophys. Res.* **82** 2040
[22] Narayana M and Sibanda P 2012 *Int. J. Heat and Mass Transfer* **55** 7552
[23] Kang H U, Kim S H and Oh J M 2006 *Exp. Heat Transfer* **19** 181
[24] Velagapudi V, Konijeti R K and Aduru C S K 2008 *Thermal Sci.* **12** 27
[25] Rudyak V Y, Belkin A A and Tomilina E A 2010 *Tech. Phys. Lett.* **36** 660
[26] Makinde O D and Aziz A 2011 *Int. J. Thermal Sci.* **50** 1326
[27] Alsaedi A, Awais M and Hayat T 2012 *Comm. Nonlinear Sci Num. Simu.* **17** 4210
[28] Kandasamy R, Muhaimin I, Khamis A B and Roslan R bin 2013 *Int. J. Thermal Sci.* **65** 196
[29] Kameswaran P K, Shaw S, Sibanda P and Murthy P V S N 2013 *Int. J. Heat Mass Transfer* **57** 465
[30] Mustafa M, Hayat T, Pop I, Asghar S and Obaidat S 2011 *Int. J. Heat Mass Transfer* **54** 5588
[31] Nandy S K and Mahapatra T R 2013 *Int. J. Heat Mass Transfer* **64** 1091
[32] Ibrahim W, Shankar B and Nandeppanavar M M 2013 *Int. J. Heat Mass Transfer* **56** 1
[33] Makinde O D, Khan W A and Khan Z H 2013 *Int. J. Heat Mass Transfer* **62** 526
[34] Ibrahim W and Shankar B 2013 *Computers and Fluids* **75** 1
[35] Zheng L, Zhang C, Zhang X and Zhang J 2013 *J. Franklin Institute* **350** 990
[36] Khan M S, Alam M M and Ferdows M 2013 *Procedia Engineering* **56** 316
[37] Liao S J 2003 (Boca Raton: Chapman and Hall/CRC Press)
[38] Abbasbandy S and Shirzadi A 2011 *Comm. Non-linear Sci. Num. Simul.* **16** 112
[39] Rashidi M M and Erfani E 2009 *Comp. Phy. Comm.* **180** 1539
[40] Hayat T, Shehzad S A, Alsaedi A and Alhothulai M S 2012 *Chin. Phys. Lett.* **29** 114704